Peer-reviewed version available at Polymers 2019, 11, 226; doi:10.3390/polym11020226

Article

Improving the supercritical CO_2 Foaming of Polypropylene by the Addition of Fluoroelastomer as a Nucleation Agent

Chenguang Yang [1,2,3,#], Quan Zhao [1,#], Zhe Xing [1], Wenli Zhang [1,2], Maojiang Zhang [1,3], Hairong Tan [1,3], Jixiang Wang[1] and Guozhong Wu [1,3,*]

[1] Shanghai Institute of Applied Physics, Chinese Academy of Sciences, Jialuo Road 2019, Jiading, Shanghai, 201800, China; yangchenguang@sinap.ac.cn (C.-G.Y.); zhaoquan@sinap.ac.cn (Q.Z); xingzhe@sinap.ac.cn (Z.X); zhangwenli@sinap.ac.cn (W.-L.Z); zhangmaojiang@sinap.ac.cn (M.-J.Z); tanhairong@sinap.ac.cn (H.-R.T); wangjixiang@sinap.ac.cn (J. –X.W)

[2] University of China Academy of Sciences, Beijing, 100049, China

[3] School of Physical Science and Technology, ShanghaiTech University, Haike Road 100, Pudong, Shanghai, 201210, China; yangchg@shanghaitech.edu.cn (C.-G.Y)

* Correspondence: wuguozhong@sinap.ac.cn;
Tel/Fax: +86-21-39194531/+86-21-39195118.

[#] These authors contributed equally to this work.

Abstract: Polypropylene (PP) foam has a great deal of application since it normally exhibits non-uniform cell size distribution, low cell density, and cracked cells. In this study, a small amount of fluoroelastomer (FKM) was used as a nucleating agent to prepare well-defined microporous PP foam by supercritical CO_2. It was observed that solid FKM was present as the nanoscale independent phase in PP matrix and the FKM could induce a mass of CO_2 aggregation, which significantly enhanced the diffusion rate of CO_2 in PP. The resultant PP/FKM foams exhibited much smaller cell size (~24 μm), and more than 16 times cell density (3.2×10^8 cells/cm^3) as well as a much more uniform cell size distribution than that of the neat PP foam. PP/FKM foams possessed major concurrent enhancement in their tensile stress and compressive stress compared to neat PP foam. We believed that the added FKM played a key role in enhancing the heterogeneous nucleation, combined with the local strain field variation in the multiple-phase system, which was responsible for the considerably improved cell morphology of PP foaming. This paper provides a deep understanding of the $scCO_2$ foaming behavior of PP in the presence of FKM.

Keywords: Polypropylene, Fluoelastomer, $scCO_2$ foaming, Heterogeneous Nucleation

1. Introduction

As a widely investigated commercial polymer, polypropylene (PP) foam has many desirable and beneficial properties, such as excellent chemical-resistance, good comprehensive mechanical properties, ease of processing, low electrical conductivity, relatively low cost and unique porous honeycomb structure [1-6]. PP foams are attractive for their wide range of various industrial applications in the fields of packaging, automobiles, aerospace, acoustic absorbent, dielectric materials, energy storage materials, thermal and thermal insulators, as well as tissue engineering [1-5,7]. However, owing to its low melt strength, melt elasticity, and high crystallinity, the fabrication of linear PP foams has not been successful [8-12]. Consequently, the resultant PP foam usually

possesses large cell diameter, non-uniform cell size distribution, and low cell density as well as poor mechanical properties.

To improve the melt strength, considerable efforts have been made to optimize the PP foaming process, enhance PP foam ability as well as improve cellular structure [11,13-23], such as long-chain branching [24,25], crosslinking [10,20,26-28], polymer blending[11,29], and compounding [30,31]. In recent years, it was found nanoparticles such as graphene, carbon nanotubes, and carbon nanofibers added in PP could provide heterogeneous nucleation sites to increase cell density, minish cell size, improve cell uniformity, and at the same time reinforce the polymeric matrix [11,22,32-34]. But the cost of these nanoparticles are high, making it difficult to use them for the high-volume production of polymer foams [11]. Moreover, the foaming behavior of polymer was greatly influenced by the solubility of CO_2 in melt polymer, which determines the cell morphology, expansion ratio, and crystallinity of the resultant foams [35-37]. Additionally, the use of supercritical fluid (SCF) can decrease the melt viscosity of the polymer during processing because of the plasticizing effect of the dissolved gas and thus can enhance the processability of polymers [11,22,35,36,38].

Thermoplastic fluoroelastomer (FKM) possesses outstanding chemical-resistant, high melt point, excellent weather resistance as well as flame retardance property. Especially, good affinity and solubility between fluorine compunds and carbon dioxide were found [39,40]. However, PP foaming by means of $scCO_2$ has not been investigated in the presence of FKM. Herein, a small amount of FKM was applied as a nucleating agent to improve the $scCO_2$ foaming of PP. The results showed that enhanced heterogeneous nucleation and increased foaming ability were obtained in the presence of FKM. The saturated mixed phases (PP/FKM/CO_2) are like an "island model", and the existence of FKM can enhance the heterogeneous nucleation during the foaming process. The obtained PP/FKM foam possessed large cell density, small cell size, uniform cell size distribution as well as excellent expansion ratio. In addition, the resultant PP/FKM foams endowed unusual tensile and compressive strength at a wide foaming pressure range. Furthermore, the foaming parameters of PP/FKM including foaming pressure and saturation time were also investigated in detail.

2. Materials and Methods

2.1. Materials

Random polypropylene (Sep-540) with a density of 0.89 g/cm^3 and a melt flow index of 7.0 g/10 min (230 °C /2.16 kg) was purchased from LOTTE Chemical Co. Fluoroelastomers (FKM 246) with a density of 1.86 g/cm^3 was purchased from Sinopec Shanghai Chemical Co. (Shanghai). Carbon dioxide with a purity of 99.95% was supplied by Xiangkun Special Gases of Shanghai.

2.2. Sample preparation

The PP pellets and FKM were vacuum-dried at 60 °C for 4 h before they were mixed. A series of mixtures of PP with FKM with contents of 0.5, 1.0, and 2.0 wt%, respectively, were made at 240 °C using a two-screw extruder (Thermo Haake PolyDrive 7, Germany). The extruded strands were cooled in water, pelletized with strand cutter. PP/FKM sheets (20 cm×20 cm) with a thickness of 1 mm were prepared by hot-pressing at 190 °C and 20 MPa, and a neat PP sheet was also prepared for comparison. The samples were coded as PP/FKM(0.5), PP/FKM(1.0), and PP/FKM(2.0), respectively. The characteristics of the PP and PP/FKM mixtures are shown in Table 1.

Table I. Characteristics of neat PP and PP/FKM mixtures.

Samples	PP	PP/FKM(0.5)	PP/FKM(1.0)	PP/FKM(2.0)
Tm /℃	165.4	165.9	166.4	167.3
XC /%	38.2	38.8	39.7	40.4

2.3. Foaming process

PP sheet samples were placed in an autoclave, and the autoclave was pressurized with CO_2 using a high-pressure liquid pump; the parameters of the foaming device have been described in the literature [10,11,20,22,23,27]. The system was kept at the preset temperature and pressure for 1 h. Then the vessel was depressurized and vented in less than 10 s. Finally, the sample was removed from the vessel and allowed to cool to room temperature.

2.4. Sample characterization

A NETZSCH STA 449 F3 Jupiter differential scanning calorimeter (DSC) equipped with a data station was used to scan the melting transitions of the samples in aluminum pans. The samples were initially heated from 25 to 230 °C at 10 °C /min under an argon flow (20 ml/min), then cooled to 30 °C at 10 °C /min, and again heated to 230 °C at the same heating rate, 10 °C/min. The first heating process was performed to eliminate the thermal history of the unfoamed samples. The melt points and melting enthalpies of the samples were obtained from the analysis software (NETZSCH-Proteus-6). The degree of crystallization was calculated using Eq. (1).

$$X_c(\%) = \frac{\Delta H_f}{\Delta H_{f0}} \times 100 \quad (1)$$

where ΔH_f is the melting enthalpy measured in the heating experiments, and ΔH_{f0} is the theoretical enthalpy of 100% crystalline PP, 207.1 J/g [35].

The morphology of the unfoamed and foamed samples was observed using a scanning electron microscope (SEM; Zeiss MERLIN Compact 14184, Germany). Samples were immersed in liquid nitrogen for 2 min, fractured, and mounted on stubs. They were then sputter-coated with gold to prevent charging during the test.

2.5. Morphological observation of the foams

The microstructural morphology of the neat PP foam and PP/FKM foam was characterized by measuring the cell density and average cell size. Image Pro-Plus software was used to analyze the SEM photographs. The average diameter D of the cells in the micrographs was calculated using Eq. (2).

$$D = \frac{\sum d_i n_i}{\sum n_i} \quad (2)$$

where n_i is the number of cells with a perimeter-equivalent diameter of d_i. To ensure the accuracy of the average pore size measurement, i is greater than 200.

The volume expansion ratio of each sample was calculated as the ratio of the density of the original sample, ϱ_s, to the measured density of the foam sample, ϱ_f. The densities (ϱ_f) of the foam samples were determined from Archimedes' law by weighing the polymer foam in water with a sinker using an electronic analytical balance (HANG-PING FA2104) and using Eq. (3) to calculate the density.

$$\varrho_f = \left(\frac{a}{a+b-c} \right) \varrho_w \quad (3)$$

where a, b, and c are the weights of the specimen in air without the sinker, the totally immersed sinker, and the specimen immersed in water with the sinker, respectively, and ϱ_w is the density of water.

The volume expansion ratio (Vf) was calculated using Eq. (4).

$$V_f = \frac{\varrho_s}{\varrho_f} \quad (4)$$

where ϱ_s and ϱ_f are the density of solid and foam samples, respectively.

The porosity P_f is related to the density of the foam ϱ_f and the unfoamed polymer ϱ_s, which was calculated using Eq. (5).

$$P_f(\%) = \left(1 - \frac{\varrho_s}{\varrho_f}\right) \times 100 \quad (5)$$

The cell density (N_0) was determined as the number of cells per unit volume of the foam, which was calculated using Eq. (6).

$$N_0 = \left(\frac{n}{A}\right)^{3/2} V_f \quad (6)$$

where n and A are the number of cells in the micrograph and the area of the micrograph (cm^2), respectively.

2.6. Mechanical properties

Tensile tests of the unfoamed and foamed samples were conducted using a universal testing machine (Instron 5943, America). The unfoamed samples were measured according to GB/T1040.2-2006/ISO 527-2:1993, and the foamed samples were cut into 2 mm × 4 mm × 25 mm pieces. All the specimens were measured at room temperature in accordance with ASTM D-638 at a speed of 50 mm/min. The compression test of the foams was performed using an MTS universal microtester equipped with a 50 N load cell. Cubic specimens with a side length of 6 mm, cutting from the foamed samples, were employed for compression tests and the speed was 1 mm/min here and more than five samples were measured for each sample at the same condition [41].

3. Results and discussion

3.1. Microscopic structure of PP/FKM blends

PP/FKM mixtures with various FKM contents were mixed by an extrusion system. To understand the dispersion of FKM in PP phase, we analyzed the SEM micrographs of PP/FKM samples. Figure 1 shows the fractured surface images of the resultant neat PP and PP/FKM mixtures. It can be easily seen that FKM has an excellent dispersion stability in PP matrix. The size of the formation dispersion phase of FKM was about 250 nm in the PP phase and it could be clearly seen that the size of FKM particles in PP matrix were all nanoscale. According to the literatures [39,40], the FKM phase is still solid state at the foaming temperature (152 °C), so the existence of FKM may play as the nucleating agent in forming cellular structure of PP during the foaming process.

Peer-reviewed version available at Polymers 2019, 11, 226; doi:10.3390/polym11020226

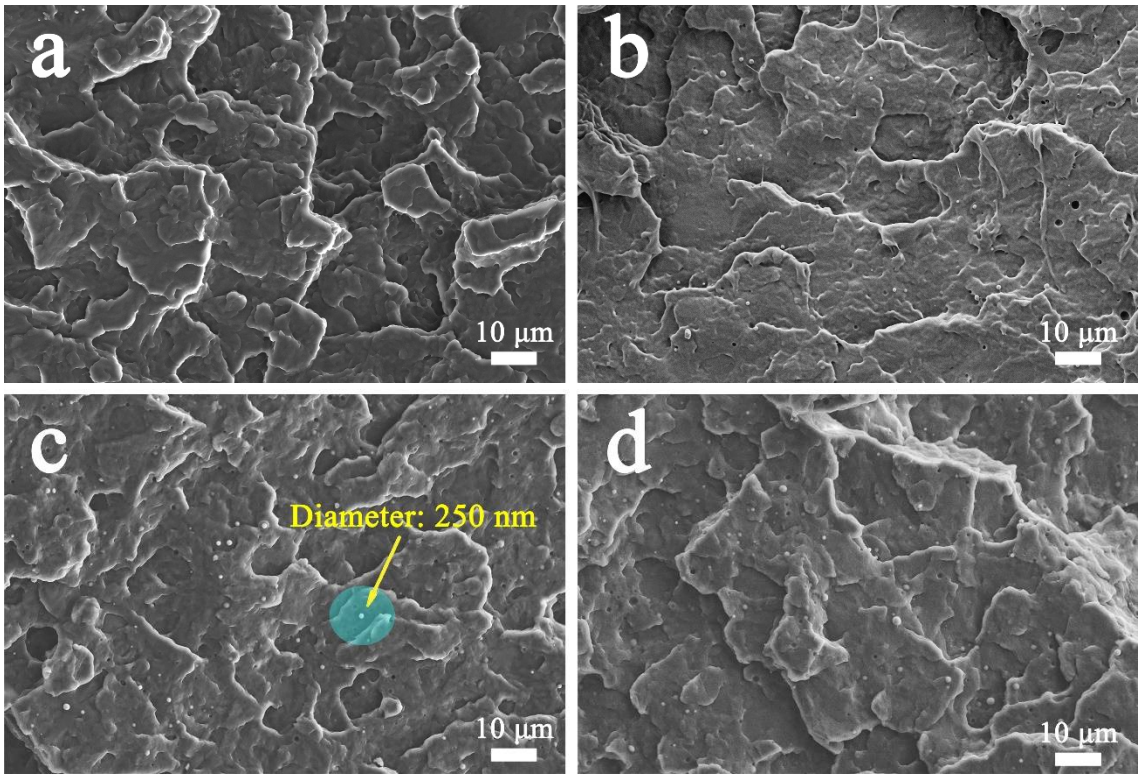

Figure 1. SEM images of fractured surfaces of (**a**) neat PP, (**b**) PP/FKM(0.5), (**c**) PP/FKM(1.0), and (**d**) PP/FKM(2.0) samples

3.2. Morphology and properties of PP/FKM foams

The cell morphologies of neat PP, PP/FKM(0.5), PP/FKM(1.0), and PP/FKM(2.0) foams prepared at 152 °C and 20 MPa are shown in Figure 2. It can be clearly seen that the cell size declined as the loading of FKM increasing. Cracked and consolidated cells appeared and the cells continuity was poor in the neat PP foam. The PP/FKM foams exhibited different cellular structure with different FKM contents. The cell size distributions of different foams are shown in Figure 2. PP/FKM foams possessed narrower cell distributions than that of the neat PP foam. Especially, PP/FKM(1.0) and PP/FKM(2.0) foams exhibited much more uniform cell size distribution. Moreover, increased porosities were obtained as the loading of FKM increasing, which indicated a much better foaming ability of PP. These results implied that the enhanced diffusion rate and increased solubility of CO_2 was obtained in the presence of FKM, resulting in a large porosity, which was also found in the previous studies about fluorinated ethylene propylene copolymer (FEP) foaming by supercritical CO_2 [42,43]. Furthermore, the independent solid-state FKM phase in PP matrix may significantly enhance the heterogeneous nucleation during the foaming process.

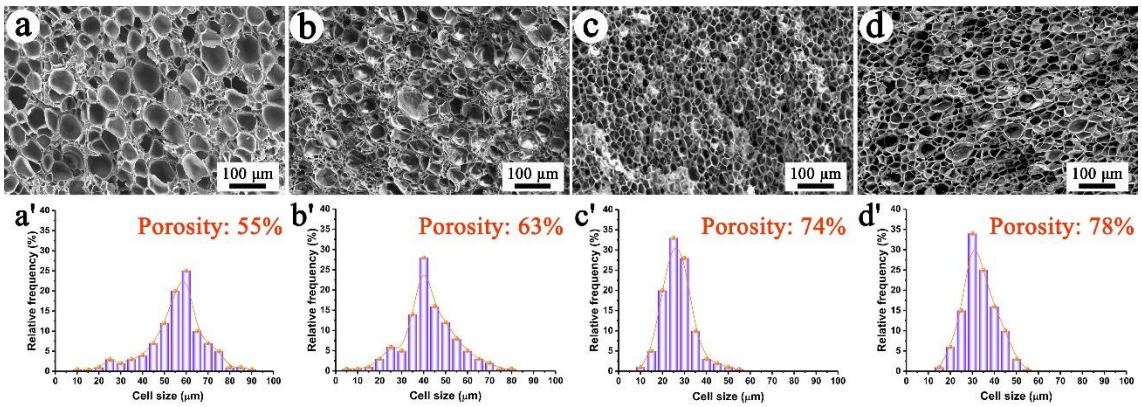

Figure 2. SEM micrographs and cell size distributions of foamed (**a**) neat PP, (**b**) PP/FKM(0.5), (**c**) PP/FKM(1.0), and (**d**) PP/FKM(2.0), all prepared at 152 °C and 20 MPa.

The average cell diameter and cell density of the cellular structure of the neat PP and PP/FKM(0.5), PP/FKM(1.0), and PP/FKM(2.0) foams are summarized in Figure 3a. The cell size of PP foams decreased from 65 to 23 μm as the loading of FKM increased from 0 to 1.0 wt% and the cell density increased significantly compared to neat PP foam, which was more than 16 times. The foam density and expansion ratio of foamed samples are shown in Figure 3b. The foam density declined as the addition content of FKM increasing from 0 to 2.0 wt%, which was consistent with the results in Figure 2. The existence of FKM led to higher diffusion rate and solubility of CO_2 in melt PP matrix and enough CO_2 could support the cell growth for long time [42,43]. According to "Heterogeneous Nucleation Theory", the formed nanoscale solid FKM phase in PP matrix can act as the nucleating agent, it is vividly shown in Figure 4. It is known that foaming is a rapid process for cells growing quickly in a few seconds, depending on the thermophysical and rheological properties of polymer/CO_2 mixtures, and this process is related to the change of temperature, pressure, and local stress, etc. In the multiple phase system (PP, FKM, and CO_2), the existence of FKM phase induces a mass of CO_2 aggregation, which is like as an "island". During the process of release pressure, it was easy to cause the change of local stress around "island", and induce large number of nucleation sites appearing, which greatly increased nucleation rate. Furthermore, the presence of large amount of cell sites caused by heterogeneous nucleation competed for the limited CO_2, which suppressed the cell growth [44]. In addition, the suitable foaming conditions of FKM were about 230 °C and 30 MPa [42]. A small amount of CO_2 might dissolve into the FKM phase in the saturation process, so it might also enhance the foaming ability of PP/FKM samples.

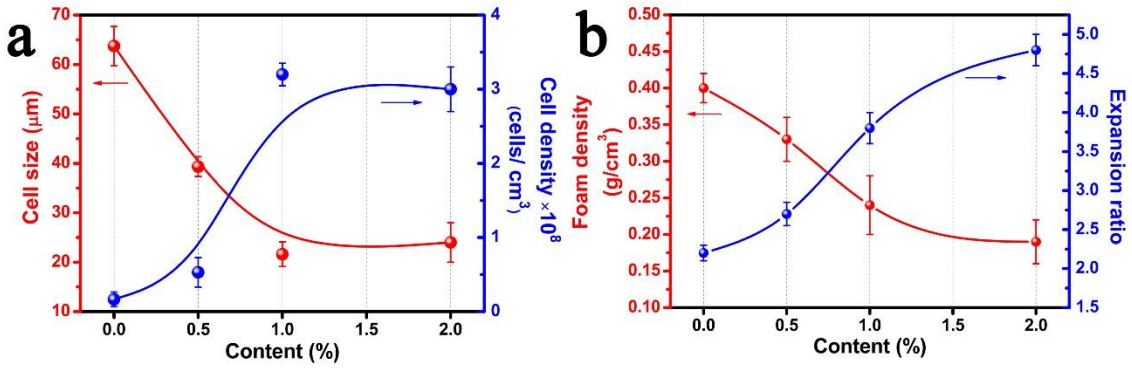

Figure 3. (**a**) Average cell diameter and cell density, (**b**) Foam density and expansion ratio of neat PP, PP/FKM(0.5), PP/FKM(1.0), and PP/FKM(2.0) foams

Peer-reviewed version available at Polymers 2019, 11, 226; doi:10.3390/polym11020226

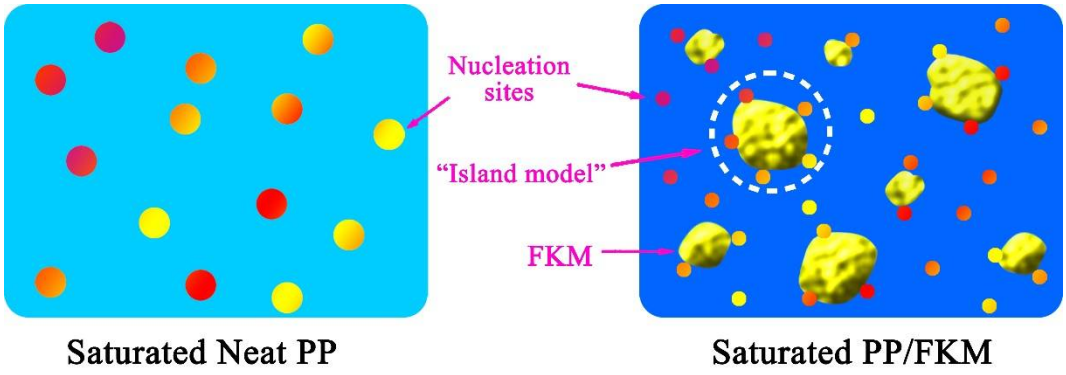

Figure 4. Schematic diagram showing the nucleation mechanism of the inner region of neat PP and PP/FKM samples. For clarity, the size of each symbol is not proportional to the real size.

The mechanical properties of resultant PP foam are the important evaluation parameters for potential industrial application. The tensile stress-strain and compressive stress-strain curves of neat PP and PP/FKM foams saturated and then foamed at 20 MPa and 152 °C are shown in Figure 5. It can be clearly seen that PP/FKM foams possess excellent stress and strain compared to neat PP foam. The tensile stress increased to more than 15 MPa and the tensile strain of PP/FKM foam was 110%. The compressive strength results showed that PP/FKM exhibited higher stress than neat PP foam. The obtained outstanding mechanical properties were ascribed to well-defined cellular structure and high continuous polygonal cell morphology of PP/FKM(1.0) foam [8,11,22,23]. All these clear results signified the key role of FKM in preparing fine PP foam with excellent mechanical properties, which indicated the promising engineering applications.

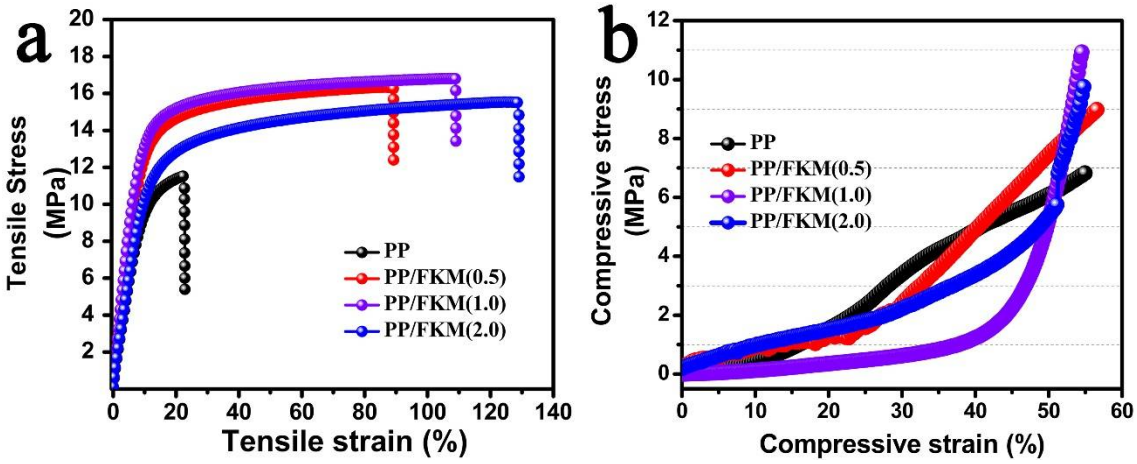

Figure 5. Mechanical properties of neat PP and PP/FKM foam samples: (**a**) tensile strength and (**b**) compressive strength.

3.3. Effects of Foaming Pressure on the Foaming Behavior of PP/FKM(1.0)

Figure 6 shows the influence of foaming pressure on the cell morphologies of PP/FKM(1.0) at 152 °C. All the samples were foamed regardless of the pressure (15, 20, and 25 MPa). However, there was a large difference in the cell morphology of neat PP foams prepared at different pressures. There were non-foamed regions and non-uniform cell size in the neat PP foam prepared at 15 MPa and it caused by insufficient swelling of CO_2. While the resultant PP/FKM(1.0) foams exhibited similar and good cellular structure at different foaming pressures.

Preprints (www.preprints.org) | NOT PEER-REVIEWED | Posted: 25 December 2018 doi:10.20944/preprints201812.0301.v1

Peer-reviewed version available at Polymers 2019, 11, 226; doi:10.3390/polym11020226

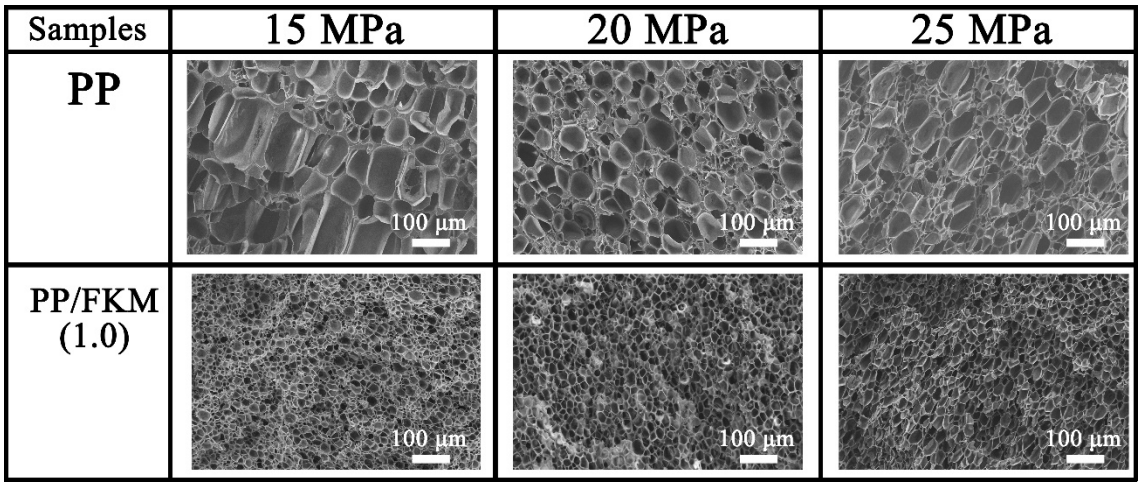

Figure 6. SEM micrographs of PP/FKM(1.0) foam prepared at 152 °C and different pressures: 15, 20, and 25 MPa.

The cell size and cell density of neat PP and PP/FKM(1.0) foams were summarized in Figure 7. It could be seen that the PP/FKM(1.0) foams showed small cell size and high cell density. In addition, the cells of PP/FKM(1.0) foams almost all exhibited good continuity at different pressures, which indicated good mechanical properties. In general, cell size increased as the pressure increasing for the enhanced expansion force of CO_2 to cell wall. Herein, we suggest that the existence of nanoscale FKM phase increased the solubility of CO_2 around the FKM "island" in PP matrix, enhancing the foaming ability of PP/FKM.

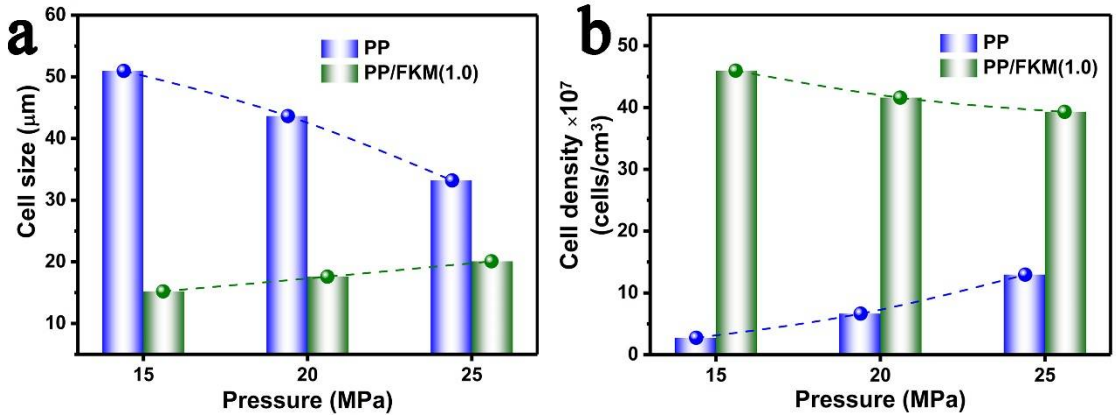

Figure 7. (**a**) Cell size and (**b**) cell density of PP/FKM(1.0) foam prepared at 152 °C and different pressures.

3.4. Effects of Saturation Time on the Foaming Behavior of PP/FKM(1.0)

From the previous discussion, the porosity of PP/FKM foams increased as the loading of FKM increasing and we ascribed it to the increased solubility of CO_2 in PP matrix. It was known that the solubility of CO_2 was also affected by the saturation time. Consequently, the influence of saturation time on cell morphology of PP/FKM(1.0) foams was also studied. It could be seen that the foaming ability of PP/FKM(1.0) was significantly enhanced as the saturation time increasing, as shown in Figure 8. Non-uniform cell size distribution and some non-foamed regions could be clearly seen in Figure 8a. The reason was that melt PP matrix was not fully saturated by CO_2 in 30 min, so it was inclined to form non-uniform distribution of cell size. More CO_2 dissolved into melt PP as the saturation time increasing, which improved the foaming ability of PP. As CO_2 continually dissolved into melt PP, the increased expansion force of CO_2 enhanced the cell growth, resulting in a larger cell size.

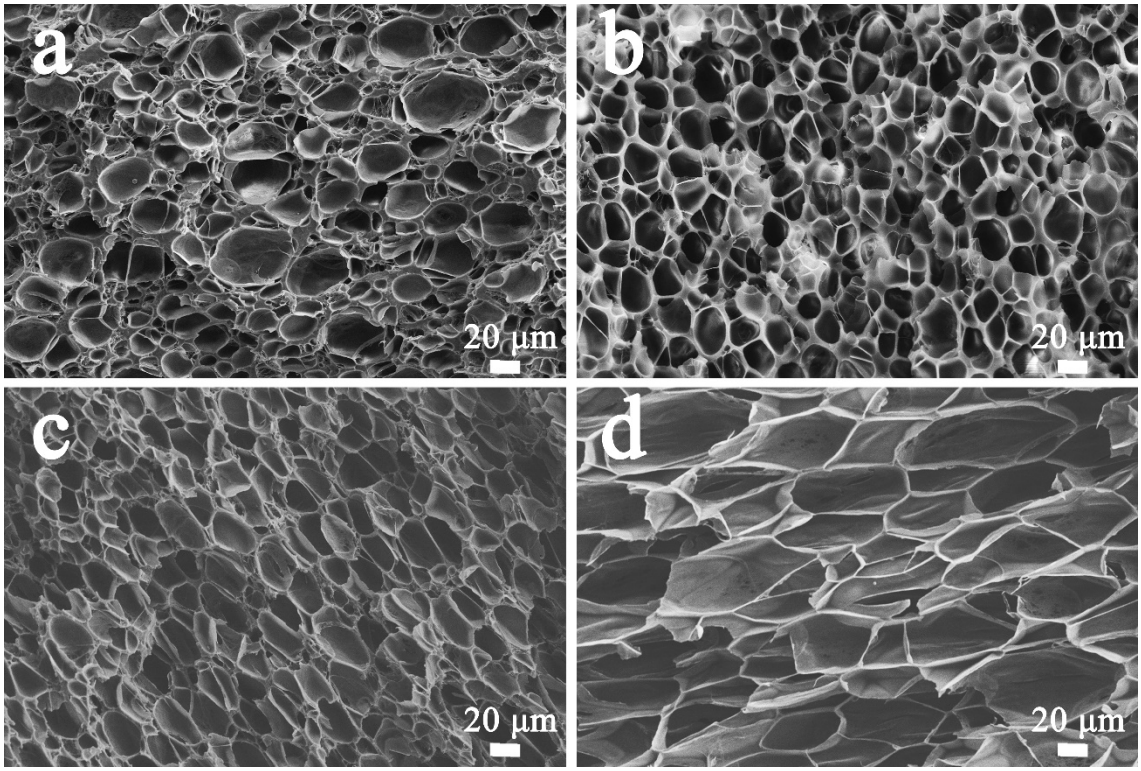

Figure 8. SEM micrographs of PP/FKM foams prepared at 152 °C and 20 MPa with different saturation time, (**a**) 30 min, (**b**) 60 min, (**c**) 90 min, and (**d**) 120 min.

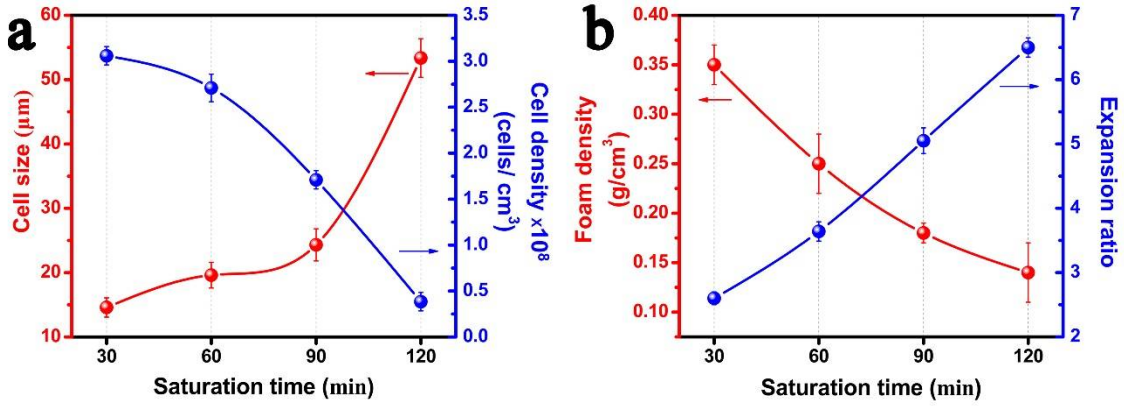

Figure 9. (**a**) Average cell diameter and cell density, (**b**) Foam density and expansion ratio of PP/FKM(1.0) foams prepared at different saturation times (30 min, 60 min, 90 min, and 120 min).

Figure 9 summarizes the parameters of the cellular structure of PP/FKM(1.0) foams as a function of saturation time. The cell size increased and the cell density decreased as the saturation time increasing from 30 to 120 min. The foam density of resultant PP/FKM(1.0) foams showed the declining phenomenon as the saturation time increasing, which indicated an increasing porosity and expansion ratio of the foams. These results indicated that the solubility of CO_2 was further increased as the saturation time increasing and large amount of CO_2 could supported cell growth. The changes of tensile stress and compressive stress of the obtained foams at different saturation times are shown in Figure 10. It is observed that the mechanical properties decrease as the saturation time increasing. Well-defined cellular structure with uniform cell size distribution and good cell continuity often exhibited good elasticity during the tensile and compressive process, resulted in unusual properties

[41,45]. These results above were well consistent with the conclusion in the previous studies [4,8,11,28,41,45].

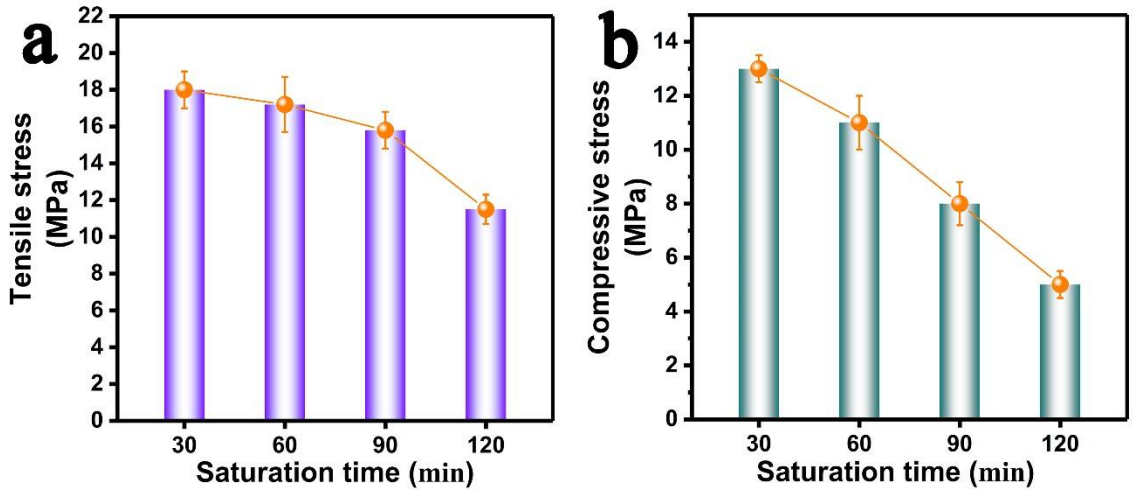

Figure 10. (**a**) Tensile stress and (**b**) compressive stress of PP/FKM foams prepared at different saturation times (30 min, 60 min, 90 min, and 120 min).

4. Conclusions

In this study, microcellular PP foam with well-defined cellular structure was fabricated in the presence of FKM by supercritical CO_2 foaming. It was found that the nanoscale solid FKM phase inducing a mass of CO_2 aggregation, which was similar to the "island model", and the FKM could greatly enhance the heterogeneous nucleation as the nucleation agent during the foaming process. The resultant PP/FKM foams exhibited smaller cell size, and more than 16 times cell density compared to neat PP foam. PP/FKM foams possessed a higher tensile and compressive stress than neat PP foam. The results also showed that FKM significantly improved the cell morphology parameters of PP/FKM foams in a large foaming pressure window. Finally, the obtained PP foams with various performance parameters could be easily controlled by changing the FKM content, foaming temperature and saturation time.

Author Contributions: conceptualization, C.-G.Y. and Q.Z.; methodology, G.-Z.W.; software, C.-G.Y.; formal analysis, C.-G.Y., Z.X. and G.-Z.W.; investigation, C.-G.Y. and J.-X.W.; resources, G.-Z.W.; data curation, Z.X. and W.-L.Z.; writing—original draft preparation, C.-G.Y. and Q.Z.; writing—review and editing, C.-G.Y., Z.X. and G.-Z.W.; visualization, H.-R.T., M.–J. Z. and Q.Z.; supervision, G.-Z.W.

Funding: This research was funded by Science Challenge Project, grant number TZ2018004.

Conflicts of Interest: The authors declare no conflict of interest.

References

1. Nofar, M.; Ameli, A.; Park, C.B. Development of polylactide bead foams with double crystal melting peaks. *Polymer* **2015**, *69*, 83-94, doi:10.1016/j.polymer.2015.05.048.
2. Hochleitner, G.; Huemmer, J.F.; Luxenhofer, R.; Groll, J. High definition fibrous poly(2-ethyl-2-oxazoline) scaffolds through melt electrospinning writing. *Polymer* **2014**, *55*, 5017-5023, doi:10.1016/j.polymer.2014.08.024.
3. Ameli, A.; Wang, S.; Kazemi, Y.; Park, C.B.; Poetschke, P. A facile method to increase the charge storage capability of polymer nanocomposites. *Nano Energy* **2015**, *15*, 54-65, doi:10.1016/j.nanoen.2015.04.004.
4. Sun, J.; Xu, J.; He, Z.; Ren, H.; Wang, Y.; Zhang, L.; Bao, J.-B. Role of nano silica in supercritical CO_2 foaming of thermoplastic poly(vinyl alcohol) and its effect on cell structure and mechanical properties. *Eur. Polym. J.* **2018**, *105*, 491-499, doi:https://doi.org/10.1016/j.eurpolymj.2018.06.009.

5. Al Tawil, E.; Monnier, A.; Nguyen, Q.T.; Deschrevel, B. Microarchitecture of poly(lactic acid) membranes with an interconnected network of macropores and micropores influences cell behavior. *Eur. Polym. J.* **2018**, *105*, 370-388, doi:https://doi.org/10.1016/j.eurpolymj.2018.06.012.
6. Zhai, W.; Park, C.B. Effect of nanoclay addition on the foaming behavior of linear polypropylene-based soft thermoplastic polyolefin foam blown in continuous extrusion. *Polym. Eng. Sci.* **2011**, *51*, 2387-2397,doi: https://doi.org/10.1002/pen.22011.
7. Yang, C.; Xing, Z.; Wang, M.; Zhao, Q.; Wang, M.; Zhang, M.; Wu, G.-Z. Better scCO2 foaming of polypropylene via earlier crystallization with the addition of composite nucleating agent. *Ind. Eng. Chem. Res.* **2018**,57,15916-15923,doi: 10.1021/acs.iecr.8b03866.
8. Bao, J.-B.; Junior, A.N.; Weng, G.-S.; Wang, J.; Fang, Y.-W.; Hu, G.-H. Tensile and impact properties of microcellular isotactic polypropylene (PP) foams obtained by supercritical carbon dioxide. *J. Supercrit. Fluid.* **2016**, *111*, 63-73,doi: https://doi.org/10.1016/j.supflu.2016.01.016.
9. Fu, D.; Chen, F.; Kuang, T.; Li, D.; Peng, X.; Chiu, D.Y.; Lin, C.S.; Lee, L.J. Supercritical CO_2 foaming of pressure-induced-flow processed linear polypropylene. *Mater. Design* **2016**, *93*, 509-513,doi: https://doi.org/10.1016/j.matdes.2016.01.012.
10. Yang, C.-G.; Wang, M.-H.; Zhang, M.-X.; Li, X.-H.; Wang, H.-L.; Xing, Z.; Ye, L.-F.; Wu, G.-Z. Supercritical CO_2 Foaming of Radiation Cross-Linked Isotactic Polypropylene in the Presence of TAIC. *Molecules* **2016**, *21*, 1660, doi:10.3390/molecules21121660.
11. Yang, C.; Xing, Z.; Wang, M.; Zhao, Q.; Wu, G. Merits of the Addition of PTFE Micropowder in Supercritical Carbon Dioxide Foaming of Polypropylene: Ultrahigh Cell Density, High Tensile Strength, and Good Sound Insulation. *Ind. Eng. Chem. Res.* **2018**, *57*, 1498-1505, doi:10.1021/acs.iecr.7b04644.
12. Cui, L.; Wang, P.; Zhang, Y.; Zhou, X.; Xu, L.; Zhang, L.; Zhang, L.; Liu, L.; Guo, X. Glass fiber reinforced and beta-nucleating agents regulated polypropylene: A complementary approach and a case study. *J. Appl. Polym. Sci.* **2018**, *135*, doi:10.1002/app.45768.
13. Dlouha, J.; Suryanegara, L.; Yano, H. The role of cellulose nanofibres in supercritical foaming of polylactic acid and their effect on the foam morphology. *Soft Matter* **2012**, *8*, 8704-8713, doi:10.1039/c2sm25909e.
14. Chen, L.; Rende, D.; Schadler, L.S.; Ozisik, R. Polymer nanocomposite foams. *J. Mater. Chem. A* **2013**, *1*, 3837-3850, doi:10.1039/c2ta00086e.
15. Pardo-Alonso, S.; Solorzano, E.; Estravis, S.; Rodriguez-Perez, M.A.; de Saja, J.A. In situ evidence of the nanoparticle nucleating effect in polyurethane-nanoclay foamed systems. *Soft Matter* **2012**, *8*, 11262-11270, doi:10.1039/c2sm25983d.
16. Istrate, O.M.; Chen, B. Relative modulus-relative density relationships in low density polymer-clay nanocomposite foams. *Soft Matter* **2011**, *7*, 1840-1848, doi:10.1039/c0sm01052a.
17. Wang, J.; Zhai, W.; Ling, J.; Shen, B.; Zheng, W.; Park, C.B. Ultrasonic irradiation enhanced cell nucleation in microcellular poly (lactic acid): a novel approach to reduce cell size distribution and increase foam expansion. *Ind. Eng. Chem. Res.* **2011**, *50*, 13840-13847, doi: 10.1021/ie201643j
18. Zhai, W.; Feng, W.; Ling, J.; Zheng, W. Fabrication of Lightweight Microcellular Polyimide Foams with Three-Dimensional Shape by CO2 Foaming and Compression Molding. *Ind. Eng. Chem. Res.* **2012**, *51*, 12827-12834, doi:10.1021/ie3017658.
19. Yang, J.; Huang, L.; Zhang, Y.; Chen, F.; Fan, P.; Zhong, M.; Yeh, S. A New Promising Nucleating Agent for Polymer Foaming: Applications of Ordered Mesoporous Silica Particles in Polymethyl Methacrylate

Supercritical Carbon Dioxide Microcellular Foaming. *Ind. Eng. Chem. Res.* **2013**, *52*, 14169-14178, doi:10.1021/ie4018447.

20. Yang, C.; Xing, Z.; Zhang, M.; Zhao, Q.; Wang, M.; Wu, G. Supercritical CO2 foaming of radiation crosslinked polypropylene/high-density polyethylene blend: Cell structure and tensile property. *Radiat. Phys. Chem.* **2017**, *141*, 276-283, doi: http://dx.doi.org/10.1016/j.radphyschem.2017.07.028.
21. Zhao, J.; Zhao, Q.; Wang, C.; Guo, B.; Park, C.B.; Wang, G. High thermal insulation and compressive strength polypropylene foams fabricated by high-pressure foam injection molding and mold opening of nano-fibrillar composites. *Mater. Design* **2017**, *131*, 1-11, doi: https://doi.org/10.1016/j.matdes.2017.05.093
22. Yang, C.G.; Wang, M.H.; Xing, Z.; Zhao, Q.; Wang, M.L.; Wu, G.Z. A new promising nucleating agent for polymer foaming: effects of hollow molecular-sieve particles on polypropylene supercritical CO_2 microcellular foaming. *RSC Adv.* **2018**, *8*, 20061-20067, doi:10.1039/c8ra03071e.
23. Yang, C.G.; Xing, Z.; Zhao, Q.; Wang, M.H.; Wu, G.Z. A strategy for the preparation of closed-cell and crosslinked polypropylene foam by supercritical CO_2 foaming. *J. Appl. Polym. Sci.* **2018**, *135*, doi:10.1002/app.45809.
24. Rodríguezpérez, M.A. Crosslinked Polyolefin Foams: Production, Structure, Properties, and Applications. *Adv. Polym. Sci.* **2005**, *184*, 55-56,doi:https://doi.org/10.1007/b136244.
25. Spitael, P.; Macosko, C.W. Strain hardening in polypropylenes and its role in extrusion foaming. *Polym. Eng. Sci.* **2004**, *44*, 2090-2100,doi:https//doi.org/10.1002/pen.20214.
26. Zhai, W.; Wang, H.; Yu, J.; Dong, J.; He, J. Cell coalescence suppressed by crosslinking structure in polypropylene microcellular foaming. *Polym. Eng. Sci.* **2010**, *48*, 1312-1321,doi:https://doi.org/10.1002/pen.21095.
27. Yang, C.; Zhe, X.; Zhang, M.; Wang, M.; Wu, G. Radiation effects on the foaming of atactic polypropylene with supercritical carbon dioxide. *Radiat. Phys. Chem.* **2017**, *131*, 35-40, doi:http://dx.doi.org/10.1016/j.radphyschem.2016.10.018.
28. Yang, C.; Xing, Z.; Zhao, Q.; Wang, M.; Wu, G. A strategy for the preparation of closed-cell and crosslinked polypropylene foam by supercritical CO_2 foaming. *J. Appl. Polym. Sci.* **2017**, *135*, 45809,doi: 10.1002/app.45809.
29. Wang, G.; Zhao, G.; Zhang, L.; Mu, Y.; Park, C.B. Lightweight and tough nanocellular PP/PTFE nanocomposite foams with defect-free surfaces obtained using in situ nanofibrillation and nanocellular injection molding. *Chem. Eng. J.* **2018**, *350*, 1-11, doi:https://doi.org/10.1016/j.cej.2018.05.161.
30. Zheng, W.G.; Lee, Y.H.; Park, C.B. Use of nanoparticles for improving the foaming behaviors of linear PP. *J. Appl. Polym. Sci.* **2010**, *117*, 2972-2979,doi:https://doi.org/10.1002/app.32253.
31. Werner, P.; Verdejo, R.; Wöllecke, F.; Altstädt, V.; Sandler, J.K.W.; Shaffer, M.S.P. Carbon Nanofibers Allow Foaming of Semicrystalline Poly(ether ether ketone). *Adv. Mater.* **2010**, *17*, 2864-2869,doi:https://doi.org/10.1002/adma.200500709.
32. Wang, L.; Zhou, H.; Wang, X.; Mi, J. Evaluation of Nanoparticle Effect on Bubble Nucleation in Polymer Foaming. *J. Phys. Chem. C* **2016**, *120*, 26841-26851, doi:10.1021/acs.jpcc.6b08723.
33. Kakroodi, A.R.; Kazemi, Y.; Nofar, M.; Park, C.B. Tailoring poly(lactic acid) for packaging applications via the production of fully bio-based in situ microfibrillar composite films. *Chem. Eng. J.* **2017**, *308*, 772-782, doi:https://doi.org/10.1016/j.cej.2016.09.130.

34. Ventura, H.; Sorrentino, L.; Laguna-Gutierrez, E.; Rodriguez-Perez, M.; Ardanuy, M. Gas Dissolution Foaming as a Novel Approach for the Production of Lightweight Biocomposites of PHB/Natural Fibre Fabrics. *Polymers* **2018**, *10*, 249, doi:10.3390/polym10030249.

35. Ji, G.; Zhai, W.; Lin, D.; Ren, Q.; Zheng, W.; Jung, D.W. Microcellular Foaming of Poly(lactic acid)/Silica Nanocomposites in Compressed CO_2: Critical Influence of Crystallite Size on Cell Morphology and Foam Expansion. *Ind. Eng. Chem. Res.* **2013**, *52*, 6390-6398, doi:10.1021/ie302281c.

36. Ren, Q.; Wang, J.; Zhai, W.; Su, S. Solid State Foaming of Poly(lactic acid) Blown with Compressed CO_2: Influences of Long Chain Branching and Induced Crystallization on Foam Expansion and Cell Morphology. *Ind. Eng. Chem. Res.* **2013**, *52*, 13411-13421, doi:10.1021/ie402039y.

37. Wong, A.; Guo, Y.; Park, C.B. Fundamental mechanisms of cell nucleation in polypropylene foaming with supercritical carbon dioxide—Effects of extensional stresses and crystals. *J. Supercrit. Fluid.* **2013**, *79*, 142-151. doi:https://doi.org/10.1016/j.supflu.2013.02.013.

38. Martín-de León, J.; Bernardo, V.; Rodríguez-Pérez, M. Low Density Nanocellular Polymers Based on PMMA Produced by Gas Dissolution Foaming: Fabrication and Cellular Structure Characterization. *Polymers* **2016**, *8*, 265. doi:10.3390/polym8070265.

39. Bonavoglia, B.; Giuseppe Storti, A.; Morbidelli, M. Modeling of the Sorption and Swelling Behavior of Semicrystalline Polymers in Supercritical CO_2. *Ind. Eng. Chem. Res.* **2006**, *45*, 4739-4750, doi:10.1021/ie050842c.

40. Solms, N.v.; Zecchin, N.; Rubin, A.; Andersen, S.I.; Stenby, E.H. Direct measurement of gas solubility and diffusivity in poly(vinylidene fluoride) with a high-pressure microbalance. *Eur. Polym. J.* **2005**, *41*, 341-348, doi:https://doi.org/10.1016/j.eurpolymj.2004.09.020.

41. Wang, L.; Hikima, Y.; Ohshima, M.; Yusa, A.; Yamamoto, S.; Goto, H. Unusual Fabrication of Lightweight Injection-Molded Polypropylene Foams by Using Air as the Novel Foaming Agent. *Ind. Eng. Chem. Res.* **2018**, *57*, 3800-3804, doi:10.1021/acs.iecr.7b05331.

42. Zirkel, L.; Jakob, M.; Munstedt, H. Foaming of thin films of a fluorinated ethylene propylene copolymer using supercritical carbon dioxide. *J. Supercrit. Fluid.* **2009**, *49*, 103-110, doi:10.1016/j.supflu.2008.11.013.

43. Deverman, G.S.; Yonker, C.R.; Grate, J.W. Thin fluoropolymer films and nanoparticle coatings from the rapid expansion of supercritical carbon dioxide solutions with electrostatic collection. *Polymer* **2003**, *44*, 3627-3632,doi: https://doi.org/10.1016/S0032-3861(03)00280-5

44. Leung, S.N.; Park, C.B.; Xu, D.; Hongbo Li, A.; Fenton, R.G. Computer Simulation of Bubble-Growth Phenomena in Foaming. *Ind. Eng. Chem. Res.* **2006**, *45*, 7823-7831,doi: 10.1021/ie060295a

45. Wang, L.; Ishihara, S.; Hikima, Y.; Ohshima, M.; Sekiguchi, T.; Sato, A.; Yano, H. Unprecedented Development of Ultrahigh Expansion Injection-Molded Polypropylene Foams by Introducing Hydrophobic-Modified Cellulose Nanofibers. *ACS Appl. Mater. Inter.* **2017**, *9*, 9250-9254,doi: 10.1021/acsami.7b01329

Sample Availability: Samples of the compounds are available from the authors.